Inorg. Chem. **2005**, *44*, 3718–3730

Self-Assembly of Chiral Coordination Polymers and Macrocycles: A Metal Template Effect on the Polymer–Macrocycle Equilibrium

Tara J. Burchell and Richard J. Puddephatt*

Department of Chemistry, University of Western Ontario, London, Canada N6A 5B7

Received January 20, 2005

The self-assembly of racemic and enantiopure binaphthyl-bis(amidopyridyl) ligands 1,1′-$C_{20}H_{12}\{NHC(=O)\text{-}4\text{-}C_5H_4N\}_2$, **1**, and 1,1′-$C_{20}H_{12}\{NHC(=O)\text{-}3\text{-}C_5H_4N\}_2$, **2**, with mercury(II) halides (HgX_2; X = Cl, Br, I) to form extended metal-containing arrays is described. It is shown that the self-assembly can lead to homochiral or heterochiral polymers or macrocycles, through self-recognition or self-discrimination of the ligand units, and the primary materials can further self-assemble through hydrogen bonding between amide substituents. In addition, the formation of macrocycles or polymers can be influenced by the presence or absence of excess mercury(II) halide, through a template effect, and mercury(II) halide inclusion complexes may be formed. In one case, an unusual polymeric compound was obtained, with 1 guest HgX_2 molecule for every 12 mercury halide units in the polymer.

Introduction

There has been great interest in combining dynamic coordination chemistry and hydrogen bonding in order to build complex metal−organic coordination polymers, macrocycles, networks, and other supramolecular architectures by self-assembly from small, easily prepared building blocks.[1−4] For example, amide groups have well-known patterns of N−H···O=C hydrogen bonding, and these groups can be used to add extra dimensionality and helicity through hydrogen bonding to the macrocylic or polymeric complexes that can be formed by self-assembly from metal ions with bis(amidopyridyl) ligands.[2−4] Because hydrogen bonding between amide groups is important in controlling the higher-order structure of proteins and other biological macromolecules, this can be considered to be a biomimetic approach to the control of the architecture of molecular materials.

An interesting extension of this approach is to study self-assembly using bis(pyridyl) ligands containing both amide functionality for hydrogen bonding and a chiral center to control helicity. In the long term, chiral molecular materials could find application in asymmetric catalysis or enantioselective separations.[5] However, at this early stage of development, it is important to learn how to control the self-assembly

* To whom correspondence should be addressed. E-mail: pudd@uwo.ca. Fax: (519)661−3022.

(1) (a) Steed, J. W.; Atwood, J. L. *Supramolecular Chemistry*; VCH: New York, 2000. (b) Holliday, B. J.; Mirkin, C. A. *Angew. Chem., Int. Ed.* **2001**, *40*, 2022. (c) Sunatsuki, Y.; Motoda, Y.; Matsumoto, N. *Coord. Chem. Rev.* **2002**, *226*, 199. (d) Balamurugan, V.; Jacob, W.; Mukjerjee, J.; Mukherjee, R. *CrystEngComm* **2004**, 396. (e) Biradha, K. *CrystEngComm* **2003**, 374. (f) Beatty, A. M. *Coord. Chem. Rev.* **2003**, *246*, 131. (g) Roesky, H. W.; Andruh, M. *Coord. Chem. Rev.* **2003**, *236*, 91. (h) Kitagawa, S.; Kawata, S. *Coord. Chem. Rev.* **2002**, *224*, 11. (i) Tadokoro, M.; Nakasuji, K. *Coord. Chem. Rev.* **2000**, *198*, 205. (j) Conerney, B.; Jensen, P.; Kruger, P. E.; Moubaraki, B.; Murray, K. S. *CrystEngComm* **2003**, 454. (k) Albrecht, M. *Chem. Rev.* **2001**, *101*, 3457.

(2) (a) Muthu, S.; Yip, J. H. K.; Vittal, J. J. *J. Chem. Soc., Dalton Trans.* **2002**, 4561. (b) Muthu, S.; Yip, J. H. K.; Vittal, J. J. *J. Chem. Soc., Dalton Trans.* **2001**, 3577. (c) Schauer, C. L.; Matwey, E.; Fowler, F. W.; Lauher, J. W. *J. Am. Chem. Soc.* **1997**, *119*, 10245. (d) Aakeröy, C. B.; Beatty, A. M. *Chem. Commun.* **1998**, 1067. (e) Aakeröy, C. B.; Beatty, A. M.; Desper, J.; O′Shea, M.; Valdés-Martínez, J. *J. Chem. Soc., Dalton Trans.* **2003**, 3956. (f) Qin, Z.; Jennings, M. C.; Puddephatt, R. J. *Chem.—Eur. J.* **2002**, *8*, 735.

(3) (a) Qin, Z.; Jennings, M. C.; Puddephatt, R. J. *Inorg. Chem.* **2001**, *40*, 6220. (b) Qin, Z.; Jennings, M. C.; Puddephatt, R. J. *Chem. Commun.* **2001**, 2676. (c) Xu, X.; James, S. L.; Mingos, M. P.; White, A. J. P.; Williams, D. J.; *J. Chem. Soc., Dalton Trans.* **2000**, 3783. (d) Kuehl, C. J.; Tabellion, F. M.; Arif, A. M.; Stang, P. J. *Organometallics* **2001**, *20*, 1956. (e) Li, G.; Song, Y.; Hou, H.; Li, L.; Fan, Y.; Zhu, Y.; Meng, X.; Mi, L. *Inorg. Chem.* **2003**, *42*, 913.

(4) (a) Burchell, T. J.; Eisler, D. J.; Jennings, M. C.; Puddephatt, R. J. *Chem. Commun.* **2003**, 2228. (b) Burchell, T. J.; Eisler, D. J.; Puddephatt, R. J. *Chem. Commun.* **2004**, 944. (c) Burchell, T. J.; Eisler, D. J.; Puddephatt, R. J. *Inorg. Chem.* **2004**, *43*, 5550.

(5) (a) Noyori, R. In *Stereocontrolled Organic Synthesis*; Trost, B. M., Ed.; Blackwell Scientific Publication: Oxford, 1994; p 1. (b) Noyori, R. *Asymmetric Catalysis in Organic Synthesis*; Wiley: New York, 1994. (c) Che, C.-M.; Huang, J.-S. *Coord. Chem. Rev.* **2003**, *242*, 97. (d) Salzer, A. *Coord. Chem. Rev.* **2003**, *242*, 59. (e) Agbossou-Niedercorn, F. *Coord. Chem. Rev.* **2003**, *242*, 145. (f) Masdeu-Bultó, A. M.; Diéguez, M.; Martin, E.; Gómez, M. *Coord. Chem. Rev.* **2003**, *242*, 159. (g) Hu, A.; Lin, W. *Org. Lett.* **2005**, *7*, 455. (h) Kesanli, B.; Lin, W. *Chem. Commun.* **2004**, 2284. (i) Hu, A.; Ngo, H. L.; Lin, W. *Org. Lett.* **2004**, *6*, 2937. (j) Hu, A.; Ngo, H. L.; Lin, W. *Angew. Chem., Int. Ed.* **2004**, *43*, 2501. (k) Hua, J.; Lin, W. *Org. Lett.* **2004**, *6*, 861. (l) Hu, A.; Ngo, H. L.; Lin, W. *J. Am. Chem. Soc.* **2003**, *125*, 11490.

10.1021/ic050097w CCC: $30.25
Published on Web 04/09/2005

process. Axially chiral 1,1′-binaphthyl groups, which are often incorporated into chiral ligands for transition metal catalysts, have recently been used as a component of chiral building blocks for synthesizing chiral coordination complexes.[6−8] Rotation about the C−C bond in the binaphthyl unit is restricted as a result of the bulkiness of the naphthyl groups, and this gives the molecules, and the ligands derived from them, a natural helicity that is retained in their metal complexes.[6−8] This pioneering work has shown great promise, and so, the 1,1′-binaphthyl unit was chosen as the chiral group to be incorporated into the bis(amidopyridyl) ligands.

To date, the majority of coordination complexes and networks containing 1,1′-binaphthyl functionalized building blocks have been prepared from enantiopure ligands, and so, they are homochiral in nature.[6,7] There are relatively few examples of the use of the *racemic* ligand in the self-assembly of chiral coordination complexes.[8−10] In general, self-assembly of oligomeric or polymeric complexes from a metal ion and a racemic ligand can give individual molecules that are homochiral, through ligand self-recognition, or heterochiral, through ligand self-discrimination.[8,10] Most commonly, crystals of both types will be racemic, containing either heterochiral molecules or equal amounts of both enantiomers of homochiral molecules. The self-assembly can, therefore, be significantly different when using racemic versus enantiopure ligands, and it should then be apparent that racemic ligands have the potential to form new and interesting solid-state architectures and molecular materials. Hence, both the enantiopure and racemic binaphthyl-bis(amidopyridyl) ligands 1,1′-$C_{20}H_{12}\{NHC(=O)\text{-}4\text{-}C_5H_4N\}_2$, **1**, and 1,1′-$C_{20}H_{12}\{NHC(=O)\text{-}3\text{-}C_5H_4N\}_2$, **2**, (Chart 1) have been studied in the self-assembly reactions with mercury(II) halides reported below. The self-assembly can lead to polymers or macrocycles, through self-recognition or self-discrimination, and the primary materials can further self-assemble through hydrogen bonding. An unexpected observation is that the selectivity for the formation of macrocycles or polymers from the reaction of HgX_2 and the 4-pyridyl ligand **1** can be influenced by the presence or absence of excess mercury(II) halide, through a template effect.[11] This polymer-to-macrocycle conversion can be considered to be the opposite of ring-opening polymerization.[12] There is evidence that suggests a similar template effect occurs in the 3-pyridyl complexes, but only the 1:1 complexes could be crystallized in this case. Template effects involving inorganic, rather than organic, guests are unusual, and we are aware of only one case with mercury(II) halide guests.[11g]

Chart 1

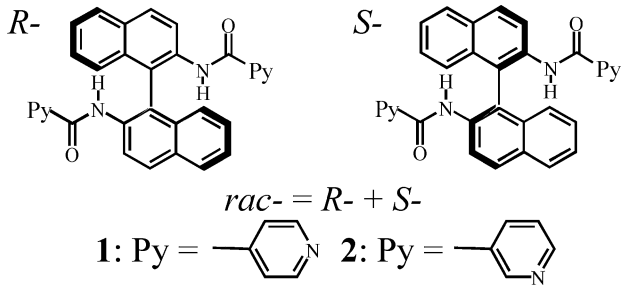

Results

Ligands *rac*-1, *R*-1, and *rac*-2. The binaphthyl-bis(amidopyridyl) ligands $C_{20}H_{12}\{NHC(=O)\text{-}4\text{-}C_5H_4N\}_2$, **1**, and $C_{20}H_{12}\{NHC(=O)\text{-}3\text{-}C_5H_4N\}_2$, **2**, were easily prepared by reaction of 1,1′-binaphthyl-2,2′-diamine, $C_{20}H_{12}(NH_2)_2$, with $4\text{-}ClC(=O)C_5H_4N\cdot HCl$ and $3\text{-}ClC(=O)C_5H_4N\cdot HCl$, respectively, and base. The ligands were prepared in the racemic forms, *rac*-**1** and *rac*-**2**, and the enantiomerically pure forms, *R*-**1** and *R*-**2** (Chart 1), by using the corresponding diamine precursor. The structure of *rac*-**1** is shown in Figure 1. The molecules of **1** associate to form a racemic mixture of homochiral supramolecular polymers [···*R*···*R*···, ···*S*···*S*···*S*···] through hydrogen bonding between NH and pyridyl groups [N(1)···N(3A) = 3.008(2) Å]. The structure of *rac*-**2** was determined previously, and in contrast to *rac*-**1**, the molecules of *rac*-**2** associate to form heterochiral polymers [···*R*···*S*···*R*···] through hydrogen bonding between NH and pyridyl groups [N(3)···N(4A) = 2.991(4) Å].[8] In both ligands, there is also an intramolecular hydrogen bond between an N−H and a C=O group of each molecule [**1**, N(2)···O(2) = 2.893(2) Å; **2**, N(2)···O(2) = 2.943(3) Å], and the presence of this secondary bond limits the span of

(6) (a) Telfer, S. G.; Kuroda, R. *Coord. Chem. Rev.* **2003**, *242*, 33. (b) Kesanli, B.; Lin, W. *Coord. Chem. Rev.* **2003**, *246*, 305.
(7) (a) Wu, C.-D.; Ngo, H. L.; Lin, W. *Chem. Commun.* **2004**, 1588. (b) Cui, Y.; Ngo, H. L.; White, P. S.; Lin, W. *Chem. Commun.* **2002**, 1666. (c) Cui, W.; Evans, O. R.; Ngo, H. L.; White, P. S.; Lin, W. *Angew. Chem., Int. Ed.* **2002**, *41*, 1159. (d) Evans, O. R.; Manke, D. R.; Lin, W. *Chem. Mater.* **2002**, *14*, 3866. (e) Cui, Y.; Lee, S. J.; Lin, W. *J. Am. Chem. Soc.* **2003**, *125*, 6014. (f) Ngo, H. L.; Lin, W. *J. Am. Chem. Soc.* **2002**, *124*, 14298. (g) Ngo, H. L.; Lin, W. *Chem. Commun.* **2003**, 1388. (h) Kesanli, B.; Cui, Y.; Smith, M. R.; Bittner, E. W.; Brockrath, B. C.; Lin, W. *Angew. Chem., Int. Ed.* **2004**, *44*, 72. (i) Lee, S. J.; Kim, J. S.; Lin, W. *Inorg. Chem.* **2004**, *43*, 6579. (j) Jiang, H.; Lin, W. *J. Am. Chem. Soc.* **2004**, *126*, 7426. (k) Lee, S. J.; Luman, C. R.; Castellano, F. N.; Lin, W. *Chem. Commun.* **2003**, *17*, 2124.
(8) Burchell, T. J.; Eisler, D. J.; Puddephatt, R. J. *J. Chem. Soc., Dalton Trans.* **2005**, 268.
(9) (a) Albrecht, M.; Schneider, M.; Röttele, H. *Angew. Chem., Int. Ed.* **1999**, *38*, 557. (b) Masood, M. A.; Enemark, E. J.; Stack, T. D. P. *Angew. Chem., Int. Ed.* **1998**, *37*, 928. (c) Krämer, R.; Lehn, J.-M.; Marquis-Rigault, A. *Proc. Natl. Acad. Sci. U.S.A.* **1993**, *90*, 5395. (d) Alkorta, I.; Elguero, J. *J. Am. Chem. Soc.* **2002**, *124*, 1488.
(10) (a) Kim, T. W.; Lah, M. S.; Hong, J.-I. *Chem. Commun.* **2001**, 743. (b) Hasenknopf, B.; Lehn, J.-M.; Baum, G.; Fenske, D. *Proc. Natl. Acad. Sci. U.S.A.* **1996**, *93*, 1397. (c) Zhou, X.-G.; Huang, J.-S.; Zhou, Z.-Y.; Cheung, K.-K.; Che, C.-M. *Inorg. Chim. Acta*. **2002**, *331*, 194. (d) Claessens, C. G.; Torres, T. *J. Am. Chem. Soc.* **2002**, *124*, 14522.
(11) (a) Dietrich-Buchecker, C.; Colasson, B.; Fujita, M.; Hori, A.; Geum, N.; Sakamoto, S.; Yamaguchi, K.; Sauvage, J.-P. *J. Am. Chem. Soc.* **2003**, *125*, 5717. (b) Mobian, P.; Kern, J. M.; Sauvage, J.-P. *J. Am. Chem. Soc.* **2003**, *125*, 2016. (c) Hamann, C.; Kern, J.-M.; Sauvage, J.-P. *Inorg. Chem.* **2003**, *42*, 1877. (d) Fuller, A. M.; Leigh, D. A.; Lusby, P. J.; Oswald, I. D. H.; Parsons, S.; Walker, D. B. *Angew. Chem., Int. Ed.* **2004**, *43*, 3914. (e) Du, M.; Bu, X.-H.; Guo, Y.-M.; Ribas, J. *Chem.−Eur. J.* **2004**, *10*, 1345. (f) Hubin, T. J.; Kolchinski, A. G.; Vance, A. L.; Busch, D. H. *Adv. Supramol. Chem.* **1999**, *5*, 237. (g) Dong, Y.-B.; Smith, M. D.; zur Loye, H.-C. *Angew. Chem., Int. Ed.* **2000**, *39*, 4271.
(12) (a) Brandys, M.-C.; Puddephatt, R. J. *Chem. Commun.* **2001**, 1280. (b) Brandys, M.-C.; Jennings, M. C.; Puddephatt, R. J. *J. Chem. Soc., Dalton Trans.* **2000**, 4601. (c) Irwin, M. J.; Vittal, J. J.; Yap, G. P. A.; Puddephatt, R. J. *J. Am. Chem. Soc.* **1996**, *118*, 13101. (d) James, S. L. *Macromol. Symp.* **2004**, *209*, 119. (e) Lozano, E.; Niewenhuyzen, M.; James, S. L.; *Chem.−Eur. J.* **2001**, *12*, 1644. (f) Miller, P.; Niewenhuyzen, M.; Charmant, J. P. H.; James, S. L. *CrystEngComm* **2004**, 408.

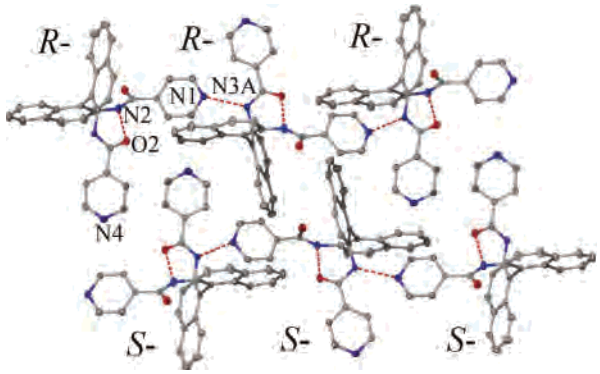

Figure 1. Chiral polymers formed by self-assembly, with self-recognition, through N−H···N hydrogen bonding between molecules in crystals of the ligand *rac*-**1**.

Scheme 1

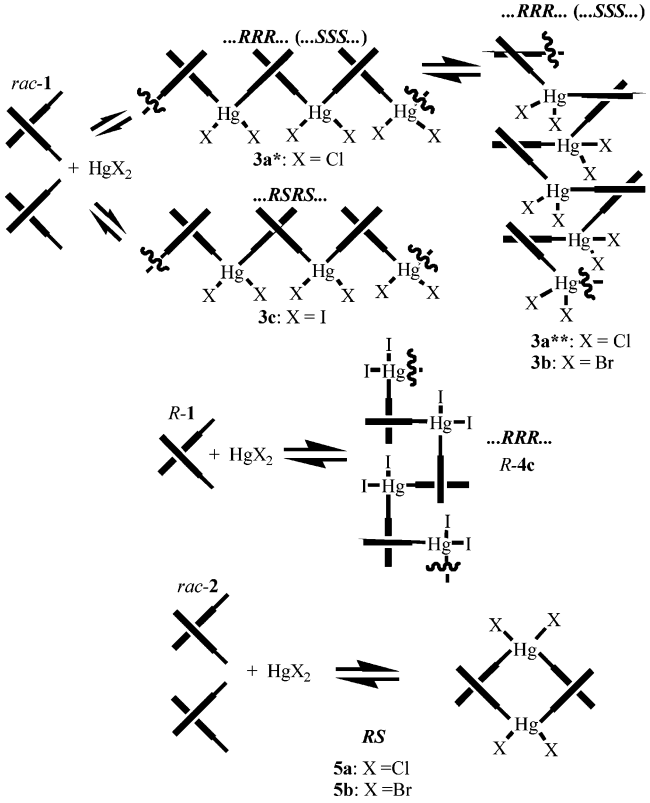

the pyridyl donors [**1**, N(1)···N(4) = 9.97 Å; **2**, N(1)···N(4) = 6.61 Å] and controls the dihedral angle between the naphthyl groups [**1**, dihedral angle = 97.2°; **2**, 97.1°]. All NH groups are involved in hydrogen bonding, whereas only half of the pyridyl and carbonyl groups are.

Polymeric and Macrocyclic Mercury(II) Halide Complexes with Ligands 1 and 2, Respectively. Reaction of equimolar amounts of the binaphthyl-bis(amidopyridyl) ligands *rac*-**1** or *R*-**1** and mercury(II) halide gave the corresponding polymers $[HgX_2(\mu\text{-}rac\text{-}\mathbf{1})]_n$, **3** (**3a**: *rac*-**1**, X = Cl; **3b**: *rac*-**1**, X = Br; **3c**: *rac*-**1,** X = I), and $[HgI_2(\mu\text{-}R\text{-}\mathbf{1})]_n$, **4c**, whereas reaction with *rac*-**2** gave the macrocycles $[(HgX_2)_2(\mu\text{-}R\text{-}\mathbf{2})(\mu\text{-}S\text{-}\mathbf{2})]$, **5** (**5a**: *rac*-**2**, X = Cl; **5b**: *rac*-**2**, X = Br) (Scheme 1). The complexes were isolated as analytically pure, air-stable, white solids that are slightly soluble in common organic solvents such as chloroform, dichloromethane, tetrahydrofuran, and methanol. Two crystalline forms of the mercury(II) chloride complex **3a** were obtained, as depicted in Scheme 1. Both can be described as containing a racemic mixture of homochiral (···*RRR*···, ···*SSS*···) polymers, but **3a*** contains zigzag polymers, whereas **3a**** contains helical polymers. The mercury(II) bromide complex **3b** is isostructural to **3a****. The mercury(II) iodide complex **3c** is fundamentally different because it crystallized as a zigzag heterochiral (···*RSRS*···) polymer. The mercury(II) chloride and bromide complexes **5a** and **5b** are isostructural and crystallized as achiral meso macrocycles. The complexes with the chiral ligands were more difficult to crystallize, and only the iodide derivative **4c** prepared from *R*-**1** was structurally characterized in the form of a helical polymer (Scheme 1). The detailed structures are discussed below.

Structures of the Coordination Polymers with Ligand 1. The structure of complex **3a*** is depicted in Figure 2, with selected bond distances and angles listed in Table 1 and hydrogen-bonding and nonbonding parameters in Table 2. In the solid state, complex **3a*** exists as a racemic mixture of homochiral zigzag polymers $[\{HgCl_2(\mu\text{-}R\text{-}\mathbf{1})\}]_n$ and $[\{HgCl_2(\mu\text{-}S\text{-}\mathbf{1})\}]_n$ in which the mercury(II) centers have roughly tetrahedral stereochemistry. In each chiral chain, successive $HgCl_2(\mu\text{-}\mathbf{1})$ units are related by a simple translation along the *c* axis (Figure 2, top). The coordinated ligands in **3a*** have a similar conformation as that in the free ligand *rac*-**1**, with both having an intramolecular N−H···O=C amide hydrogen bond. The dihedral angle between the naphthyl groups is essentially the same in **3a*** as in *rac*-**1,** whereas the distance between the nitrogen donor atoms of the pyridyl groups in **3a*** is slightly greater than that in the free ligand (Table 2). Adjacent ···*RRR*··· and ···*SSS*··· polymer chains further self-assemble through intermolecular N−H···O=C hydrogen bonds between ligands of opposite chirality (···*R*···*S*···) [N(3)···O(1A) = 2.837(5) Å] to give a two-dimensional sheet structure (Figure 2, middle). In addition, pairs of ···*RRR*··· and ···*SSS*··· chains from adjacent sheets form double-stranded polymers through weak Hg···O interactions [Hg(1)···O(2A) = 3.168 Å], and these secondary bonds link the sheets together to form a three-dimensional network (Figure 2, bottom).

The structure of complex **3a****, which is a supramolecular isomer of complex **3a***, is shown in Figure 3, and selected parameters are listed in Tables 1 and 2. In the solid state, complex **3a**** exists as a racemic mixture of polymers, $[\{HgCl_2(\mu\text{-}R\text{-}\mathbf{1})\}]_n$ and $[\{HgCl_2(\mu\text{-}S\text{-}\mathbf{1})\}]_n$, but the polymers form chiral helical chains with a pitch of 11.73 Å (Table 2), and the associated channels, rather than the zigzag chains in **3a***, and the helical channels are filled with dichloromethane guest molecules (Figure 3, top). The conformation of the ligands in **3a**** is similar to, but less open than, the conformation of the ligands in **3a***. The intramolecular amide hydrogen bond, bipyridyl group bite distance, Hg···Hg separation, and dihedral angle are all smaller than the corresponding bond lengths and angles of **3a*** (Table 2). The helical chains are further associated through intermolecular hydrogen bonding between amide groups of ligands of

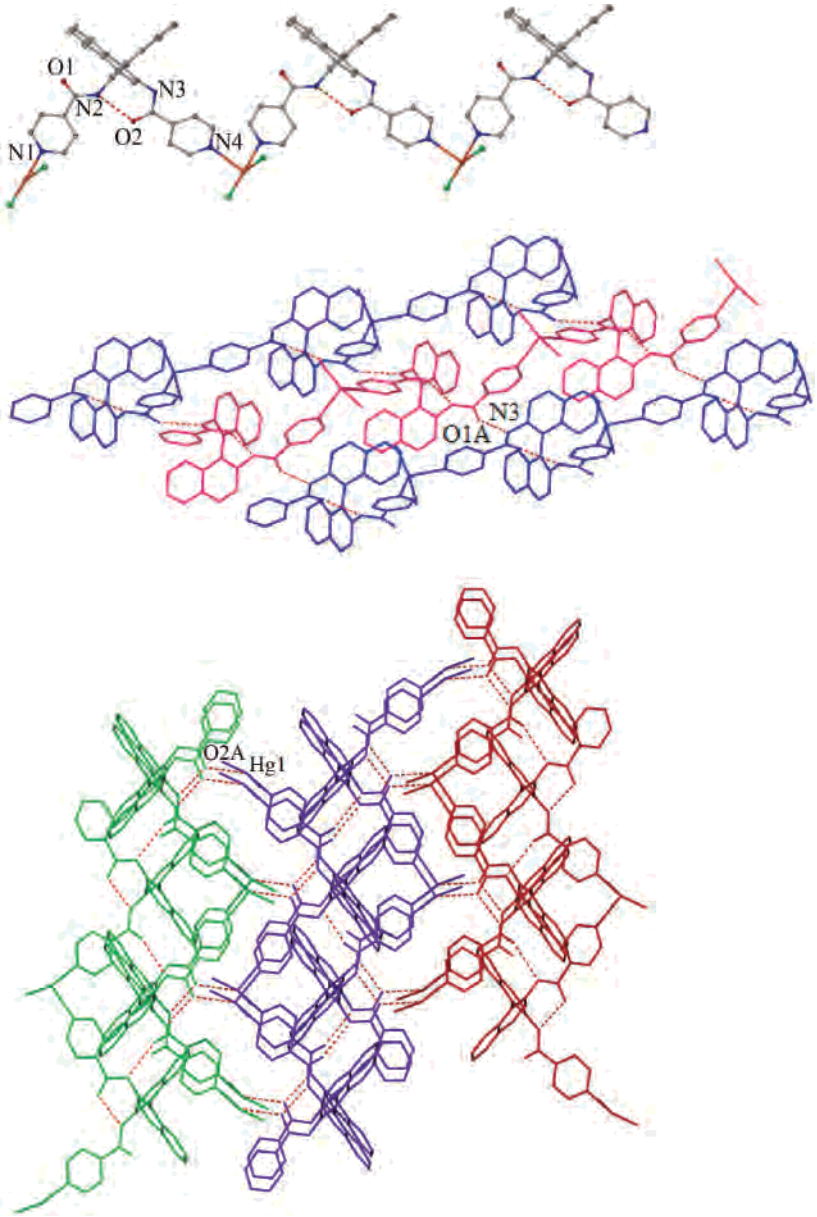

Figure 2. Solid-state structure of complex **3a***. (Top) Homochiral ···*RRR*··· chain of **3a***. (Middle) Sheet structure formed by ···*R*···*S*···*R*··· amide hydrogen bonding between ···*RRR*··· (pink) and ···*SSS*··· (blue) chains. (Bottom) Three-dimensional network formed by linking ···*R*···*S*···*R*··· hydrogen bonded sheets through Hg···O interactions (each ···*R*···*S*···*R*··· sheet is a different color).

Table 1. Selected Bond Distances (Å) and Angles (deg) for Polymer Complexes **3a***, **3a****, **3b**, **3c**, and **4c**

	3a*	**3a****	**3b**	**3c**	**4c**
Hg(1)−N(1)	2.516(4)	2.393(6)	2.396(6)	2.467(12)	2.445(7)
Hg(1)−N(4A)	2.482(4)	2.404(6)	2.407(6)	2.400(13)	2.502(6)
Hg(1)−X(1)	2.3283(14)	2.378(2)	2.4558(10)	2.6447(17)	2.6160(7)
Hg(1)−X(2)	2.3289(15)	2.335(2)	2.4992(11)	2.6628(16)	2.6316(8)
N(1)−Hg(1)−N(4A)	91.83(15)	96.9(2)	98.2(2)	95.0(4)	81.7(2)
N(1)−Hg(1)−X(1)	100.10(11)	92.33(15)	106.50(14)	97.0(3)	101.21(14)
N(4A)−Hg(1)−X(1)	98.94(11)	93.38(15)	110.42(16)	100.7(3)	101.30(14)
N(1)−Hg(1)−X(2)	93.81(11)	104.93(15)	96.62(15)	100.3(3)	100.77(15)
N(4A)−Hg(1)−X(2)	94.22(11)	110.04(15)	94.33(17)	100.2(3)	101.71(14)
X(1)−Hg(1)−X(2)	160.47(5)	148.51(8)	144.86(4)	151.45(5)	150.11(3)

opposite chirality (···*R*···*S*···) [N(1A)···O(3) = 2.827(7) Å] and form a sheet of chiral helical channels (Figure 3, bottom).

The bromide complex **3b** is isostructural with the corresponding chloride complex **3a****, and comparative structural data are included in Tables 1 and 2. As expected, the intraligand amide hydrogen bond, bipyridyl bite distance, Hg···Hg separation, dihedral angle, and pitch of the helix are very similar to those of **3a**** (Table 2), and the chiral chains self-assemble through hydrogen bonding between amide groups of enantiomeric ligands (···*R*···*S*···) [N(3)···O(1) = 2.835(7) Å] in the same way as in **3a****, forming two-dimensional sheets with internal channels.

Table 2. Intraligand N−H···C═O Hydrogen Bonds, Bipyridyl Bite Distances (N···N), Hg···Hg Separations, Dihedral Angles, and Pitches of the Helix

	N··O (Å)	N···N (Å)	Hg···Hg (Å)	dihedral angle (°)	pitch (Å)
rac-**1**	2.893(2)	9.97		97.2	
rac-**2**	2.943(3)	6.61		97.1	
3a*	2.894(5)	10.21	13.62	97.4	
3a**	2.822(7)	9.55	12.94	93.4	11.73
3b	2.823(7)	9.51	12.85	93.1	11.94
3c	2.828(16)	10.10	13.68	86.8	
4c	2.849(8)	10.19	13.53	98.8	15.58
5a	2.778(8)	7.49	9.01	92.1	
5b	2.780(9)	7.62	9.16	95.3	
6b	2.839(13)	9.96	13.26	92.7	
6c	2.87(2)	9.94	13.31	92.1	
7c	2.89(3), 2.82(3)	9.17, 9.73	11.95, 13.03	106.7, 95.7	

The structure of complex **3c** is depicted in Figure 4, and selected bond distances and angles are listed in Tables 1 and 2. In the solid-state, complex **3c** exists as a heterochiral ···*RSRS*··· polymer [{$(HgI_2)_2$(*μ*-*R*-**1**)(*μ*-*S*-**1**)}]$_n$ (Figure 4, top). The ligands of **3c** have a similar intramolecular amide hydrogen bond, bipyridyl bite distance, and Hg···Hg separation to those of **3a***, but they have a much smaller dihedral angle between the naphthyl groups (Table 2). In addition,

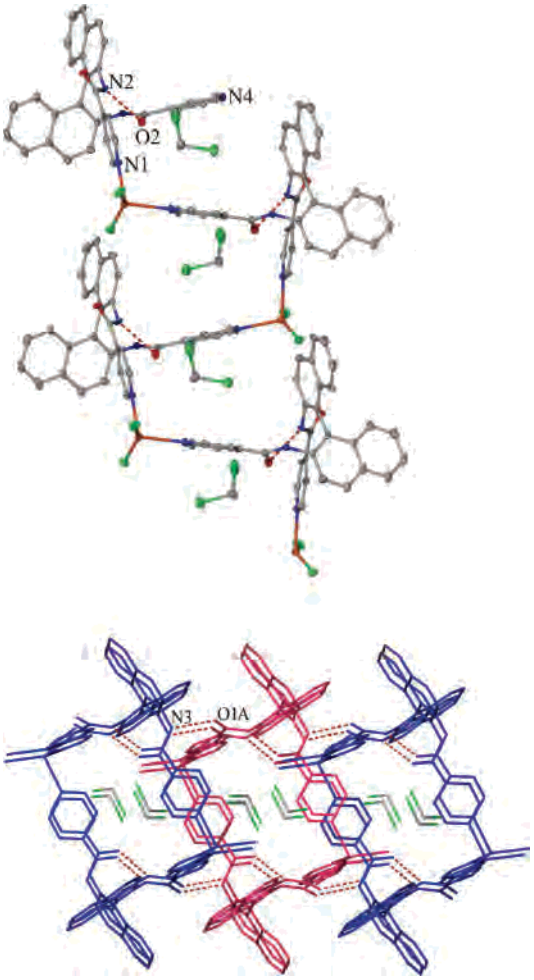

Figure 3. Solid-state structure of complex **3a****. (Top) Homochiral ···*RRR*··· helical chain of **3a**** with CH_2Cl_2 guest molecules. (Bottom) Part of the sheet structure, with internal chiral helical channels, formed by ···*S*···*R*···*S*··· amide hydrogen bonding between ···*RRR*··· (pink) and ···*SSS*··· (blue) helical strands.

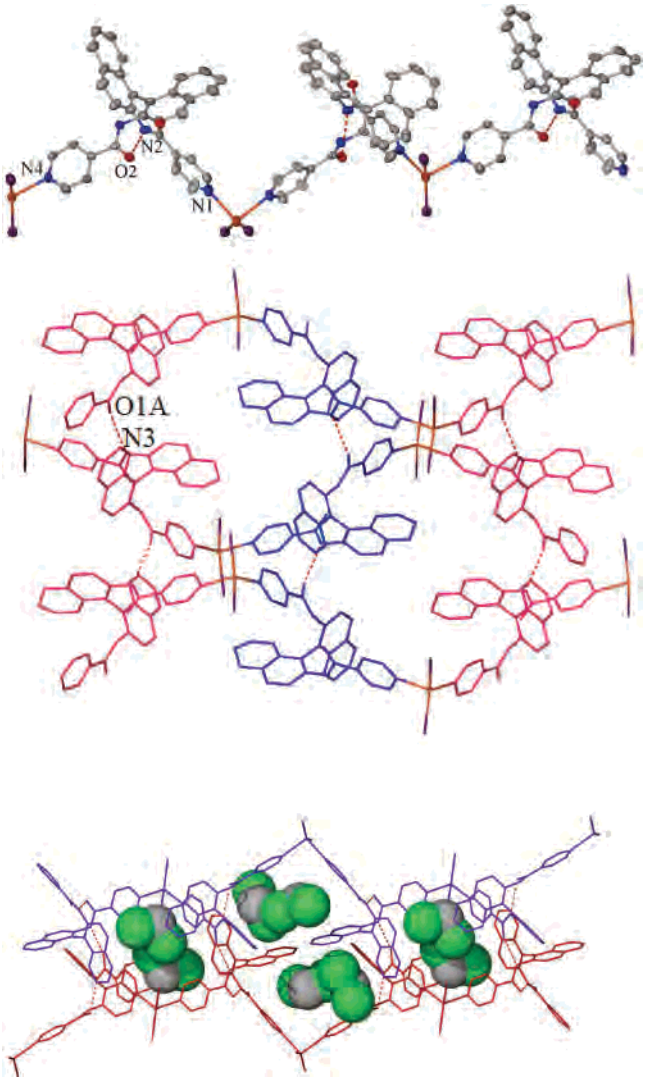

Figure 4. Solid-state structure of complex **3c**. (Top) View of a heterochiral ···*RSRS*··· polymer chain. (Middle) The two-dimensional sheet formed by ···*R*···*R*··· (pink) and ···*S*···*S*··· (blue) amide hydrogen bonding. (Bottom) View of the solvent encapsulated within the cavities formed by hydrogen bonding between two polymer chains.

there is an additional twist to the polymer chains of **3c** when compared to **3a***. In contrast to the previous examples, the association of chains of **3c** occurs through hydrogen bonding between amide groups of ligands of *like* chirality (···*R*···*R*···, ···*S*···*S*···) [N(3)···O(1A) = 2.925(16) Å] to form a two-dimensional sheet of polymers (Figure 4, middle). Furthermore, the association of polymer chains through hydrogen bonding creates small pockets in the sheet structure in which dichloromethane solvent molecules are encapsulated (Figure 4, bottom).

The structure of the enantiopure complex **4c** is depicted in Figure 5, and selected parameters are listed in Tables 1 and 2. In the solid state, the HgI_2 complex **4c** exists as helical chiral polymers [{HgI_2(*μ*-*R*-**1**)}]$_n$ (Figure 5, top) that further associate with four other chains through intermolecular amide hydrogen bonding [N(3)···O(1A) = 2.856(8) Å] to form a three-dimensional network (Figure 5, bottom). The structure is obviously different from that of the racemic HgI_2 complex **3c**, and there are also major differences with the structures

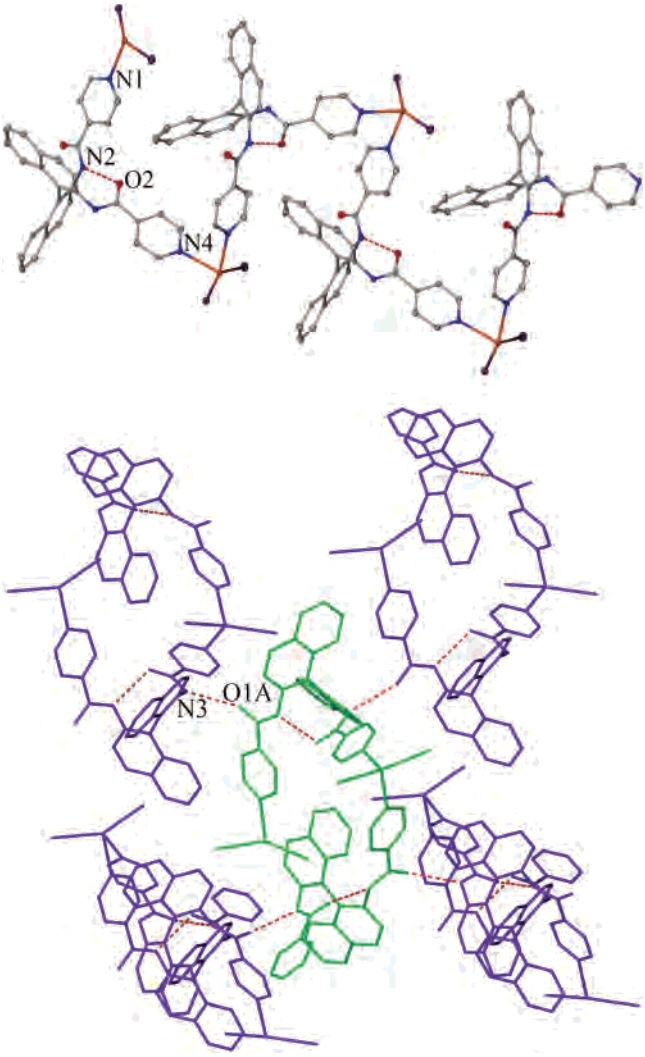

Figure 5. Solid-state structure of complex **4c**. (Top) View of the chiral helical polymer **4c**. (Bottom) Each polymer strand (green) is linked to four other strands (purple) through amide hydrogen bonds to form a three-dimensional network.

of **3a**** and **3b**, although they also contain individual helical and homochiral polymer chains. The intraligand hydrogen bond in **4c** is similar to that found in complexes **3a**** and **3b** (Table 2), but the ligand bite distance, Hg···Hg separation, and binaphthyl dihedral angle are greater in **4c** than in **3a**** and **3b**. In addition, the helical coils of **4c** have a greater pitch (15.58 Å) and are more elongated compared to those of **3a**** and **3b**, and adjacent coils are more tightly packed. Thus, if the *R*-**1** ligand is considered to contain two naphthyl-(amidopyridyl) arms, one above the other, then the mercury atoms in the polymers **3a**** and **3b** are coordinated to a top arm of one ligand and a bottom arm of another, leaving a space between, whereas the mercury atoms in **4c** are coordinated to two top arms or two bottom arms, and there is little space between neighboring units. Thus, in **3a****, there is interpenetration of neighboring helical coils and solvent inclusion in the coils (Figure 3), whereas in **4c**, there is no interpenetration of coils and no solvent inclusion (Figure 5).

Structures of the Macrocycles with Ligand 2. The structure of complex **5a** is shown in Figure 6, and selected parameters are listed in Tables 2 and 3. In the solid-state,

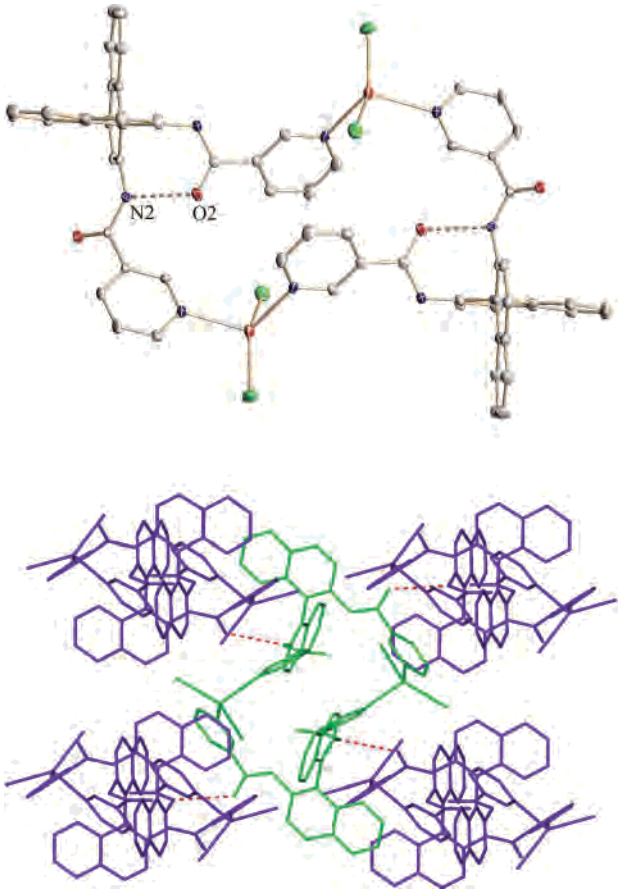

Figure 6. Solid-state structure of complex **5a**. (Top) View of the achiral meso macrocycle **5a**. (Bottom) Each macrocycle (green) is linked to four other macrocycles (purple) through amide hydrogen bonds to form a two-dimensional sheet of rings.

complex **5a** exists as a 30-membered meso macrocycle [$(HgCl_2)_2$(μ-*R*-**1**)(μ-*S*-**1**)] that contains two tetrahedral $HgCl_2$ units and one of each enantiomer of ligand **2** (Figure 6, top). There is a crystallographic inversion center at the midpoint of the macrocycle. The distance between nitrogen donor atoms of the pyridyl groups of the coordinated ligands in **5a** is larger than that in the free ligand *rac*-**2,** whereas the dihedral angle between the naphthyl groups and the intramolecular N−H···O═C hydrogen bonds are slightly smaller in complex **5a** than in the free ligand *rac*-**2** (Table 2). The cavity formed by the macrocycle is long and narrow, and there is no room for a guest solvent molecule. Each macrocycle further associates with four other macrocycles through intermolecular amide hydrogen bonding between enantiomeric ligands (*R*···*S*) [N(3)···O(1A) = 2.898(8) Å] to form a two-dimensional sheet of achiral rings (Figure 6, bottom). In these sheets, the more polar $HgCl_2$ and pyCONH units lie within the sheet, whereas the less polar binaphthyl groups form a sheath on either side.

The bromide complex **5b** is isostructural with the corresponding chloride complex **5a**. The structural features of **5b** are similar to those of **5a**, and comparative structural data are included in Tables 2 and 3.

Formation and Structure of Macrocyclic Complexes with HgX_2 Guests. Crystallization of complexes **3b** and **3c** in the presence of a large excess of mercury halide resulted

Table 3. Selected Bond Distances (Å) and Angles (deg) for the Macrocyclic Complexes **5a** (X = Cl) and **5b** (X = Br)

	5a	5b		5a	5b
Hg(1)−N(1)	2.381(7)	2.407(6)	N(1)−Hg(1)−X(1)	101.01(17)	105.84(19)
Hg(1)−N(4A)	2.416(7)	2.423(7)	N(4A)−Hg(1)−X(1)	107.61(17)	90.3(2)
Hg(1)−X(1)	2.356(2)	2.474(3)	N(1)−Hg(1)−X(2)	99.30(17)	100.49(17)
Hg(1)−X(2)	2.383(2)	2.442(2)	N(4A)−Hg(1)−X(2)	90.99(16)	113.54(19)
N(1)−Hg(1)−N(4A)	109.2(2)	107.6(2)	X(1)−Hg(1)−X(2)	145.90(9)	136.82(10)

Scheme 2

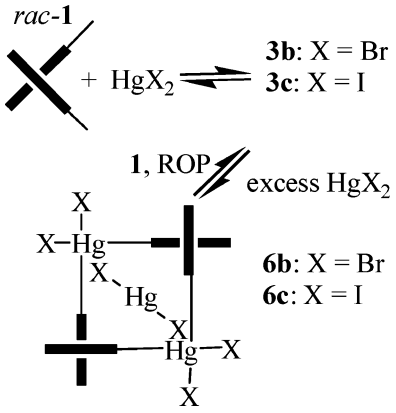

in the conversion of the polymers into 34-membered meso macrocycles $[(HgX_2)_2(\mu\text{-}R\text{-}\mathbf{1})(\mu\text{-}S\text{-}\mathbf{1})]\cdot HgX_2$ (**6b**, X = Br; **6c**, X = I; Scheme 2) that encapsulate a single linear mercury(II) halide molecule inside the ring.

The structure of complex **6b** is shown in Figure 7, with selected bond distances and angles listed in Table 4 and secondary bonding or nonbonding parameters in Table 2. Complex **6b** crystallizes as a 34-membered macrocycle of the form $[(HgBr_2)_2(\mu\text{-}R\text{-}\mathbf{1})(\mu\text{-}S\text{-}\mathbf{1})]$ with a linear $HgBr_2$ molecule at the center (Figure 7). Each macrocycle exists in the meso (*R*, *S*) form, containing one ligand *R*-**1**, one ligand *S*-**1**, and two $HgBr_2$ units, with roughly tetrahedral stereochemistry at each mercury(II) center. The conformations of the ligands in macrocycle **6b** and polymer **3b** are similar, with each having an intramolecular amide hydrogen bond and similar nonbonding parameters (Table 2). The shape of the cavity formed in **6b** is more square, rather than long and narrow as in complexes **5a** and **5b**, and it accommodates a guest molecule. The linear $HgBr_2$ guest molecule is positioned at the center of the ring, with nonbonding Hg···Hg distances of 6.63 Å and its molecular axis tilted at an angle of approximately 40° with respect to the plane of the macrocycle. There is a good fit of the linear mercury halide molecule inside the cavity of the ring, as shown by the space-filling diagram (Figure 7). There are likely secondary bonding interactions between the mercury atom of the guest molecule and the carbonyl oxygen atoms of the ring [Hg(2)···O(2) = 3.003 Å] and between the bromine atoms of the guest molecule and pyridyl groups (Figure 7).

Each macrocycle is further associated with four other rings through intermolecular amide hydrogen bonds between enantiomers (···*R*···*S*···) [N(3)···O(1A) = 2.825(12) Å], and this gives rise to a two-dimensional sheet structure similar to those found for **5a** and **5b** (Figure 8, top). However, for complex **6b**, the guest molecules are held in the center of the sheet and line up in channels with individual molecules separated by 16.22 Å, as shown in Figure 8, bottom.

The iodide complex **6c** is isostructural with the corresponding bromide complex **6b**. All features of the structures are similar, and comparative structural data are included in Tables 2 and 4.

Formation and Structure of a Polymer with HgI_2 Guests. Crystallization of complex **3c** in the presence of a small excess of mercury(II) iodide gave the unusual polymeric compound **7c**, having the stoichiometry $[\{(HgI_2)(\mu\text{-}\mathbf{1})\}_{12}]_n\cdot(HgI_2)_n$ (Scheme 3), with 1 guest HgI_2 molecule for every 12 $[HgI_2.\mu\text{-}\mathbf{1}]$ units. In this intricate network material, six polymer chains surround each guest HgI_2 molecule, as shown schematically in Scheme 3.

The structure of complex **7c** is shown in Figure 9, and selected parameters are listed in Tables 2 and 5. Complex **7c** exist as a one-dimensional heterochiral polymer $[\{(HgI_2)_2(\mu\text{-}R\text{-}\mathbf{1})(\mu\text{-}S\text{-}\mathbf{1})\}]_n$ with tetrahedral mercury(II) centers bridged by alternating enantiomers of the ligand *rac*-**1**. The individual

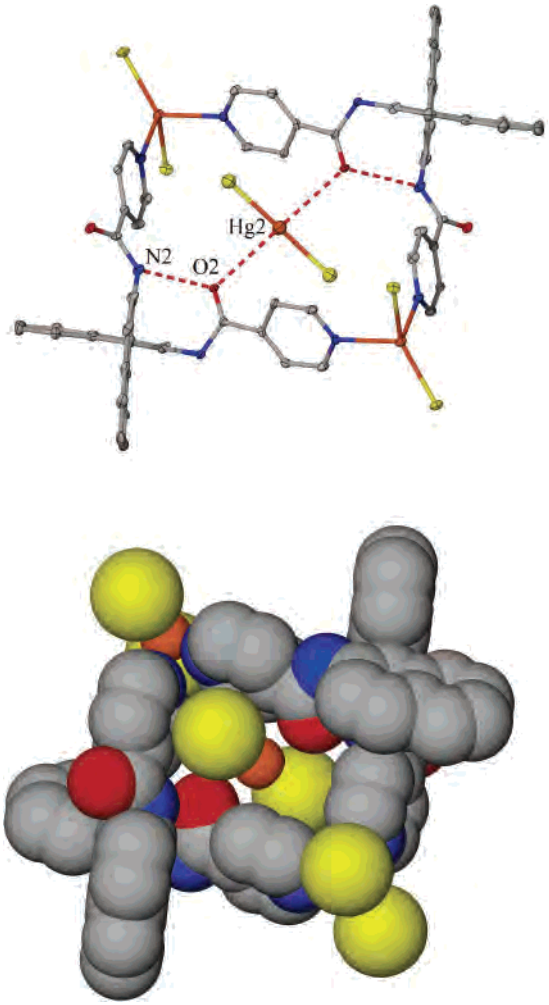

Figure 7. Structure of the macrocyclic complex **6b** with a linear $HgBr_2$ guest, showing the overall structure and a space-filling diagram.

Table 4. Selected Bond Distances (Å) and Angles (deg) for the Macrocyclic Complexes **6b** and **6c**

	6b	6c		6b	6c
Hg(1)−N(1)	2.370(10)	2.445(16)	N(1)−Hg(1)−X(1)	113.1(3)	101.8(4)
Hg(1)−N(4A)	2.435(10)	2.421(16)	N(4A)−Hg(1)−X(1)	104.8(2)	99.0(4)
Hg(1)−X(1)	2.474(3)	2.6602(16)	N(1)−Hg(1)−X(2)	98.5(3)	102.4(4)
Hg(1)−X(2)	2.5068(15)	2.6281(17)	N(4A)−Hg(1)−X(2)	95.7(2)	113.8(4)
Hg(2)−X(3)/(3A)	2.3868(17)	2.553(3)	X(1)−Hg(1)−X(2)	143.43(11)	141.13(6)
N(1)−Hg(1)−N(4A)	84.9(4)	82.7(6)	X(3)−Hg(2)−X(3A)	180.0	180.0

polymer chains of **7c** are very similar to those of polymer **3c**, with only slight differences in the nonbonding distances and dihedral angles of the ligands (Table 2). However, complex **7c** contains 1 guest molecule of HgI_2 for every 12 mercury(II) centers in the polymer chains (overall ratio **1**:Hg = 1:1.083), and alternating ligands of each chain form weak interactions with these linear HgI_2 guest molecules [Hg(3)···O(2) = 3.4 Å] such that, in one chain, each *S*-**1** ligand associates with a molecule of HgI_2 and, in another chain, each *R*-**1** ligand is involved in the O···Hg interaction. Furthermore, three pairs of parallel polymer chains surround each linear HgI_2 molecule (Figure 9, top), and the chains intertwine and associate through intermolecular amide hydrogen bonds [N(2)···O(3A) = 2.88(3) Å, N(7)···O(4) = 3.10(3) Å] such that a three-dimensional grid structure is formed (Figure 9, middle and bottom).

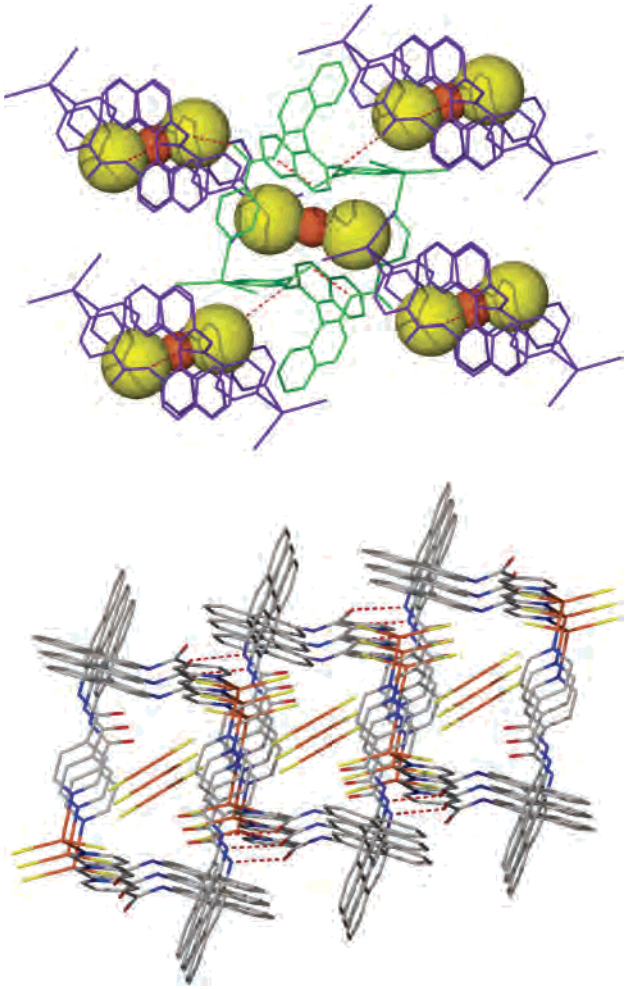

Figure 8. (Top) The sheet structure of **6b** formed by association of macrocycles through ···*R*···*S*··· amide hydrogen bonds. (Bottom) The channels within each sheet that contain the guest molecules.

Scheme 3

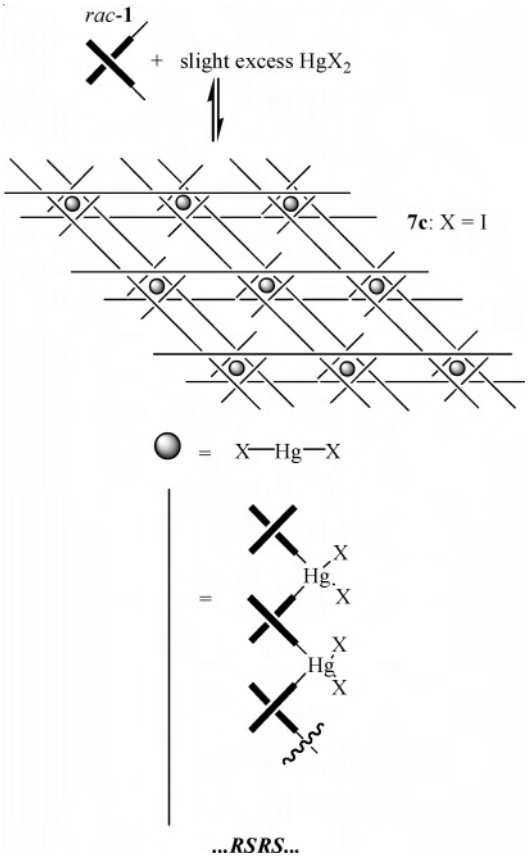

NMR Studies of the Complexes in Solution. Complexes **3**−**5** were characterized by ^{1}H NMR spectroscopy, with chemical shifts tabulated in Tables 6 and S1 (Supporting Information), on the basis of the labeling schemes shown in Chart 2. The ^{1}H NMR spectra of the 4-pyridyl mercury halide complexes **3** and **4** in CD_2Cl_2 solution are similar to each other, as are the spectra of the 3-pyridyl complexes **5**, but there are significant coordination shifts. In particular, the N−H and pyridyl proton resonances of complexes **3** and **4** display significant coordination shifts compared to those of the free ligand **1** (Table 6). Only one resonance was observed for each hydrogen atom of Chart 2, but it is not clear if this arises from dynamic exchange between oligomers or if there are only simple molecules, such as macrocycles, present.

Upon addition of excess mercury halide to solutions of the 1:1 complexes **3**−**5** in CD_2Cl_2, significant changes to the ^{1}H NMR spectra were observed (Table 6 and Table S1 in the Supporting Information). For example, the chemical shifts of protons A and P of the naphthyl rings of the 4-pyridyl complexes **3** and **4** decrease and increase, respectively, and the N−H resonance and pyridyl proton resonances all increase (Table 6). Similar changes were observed in the

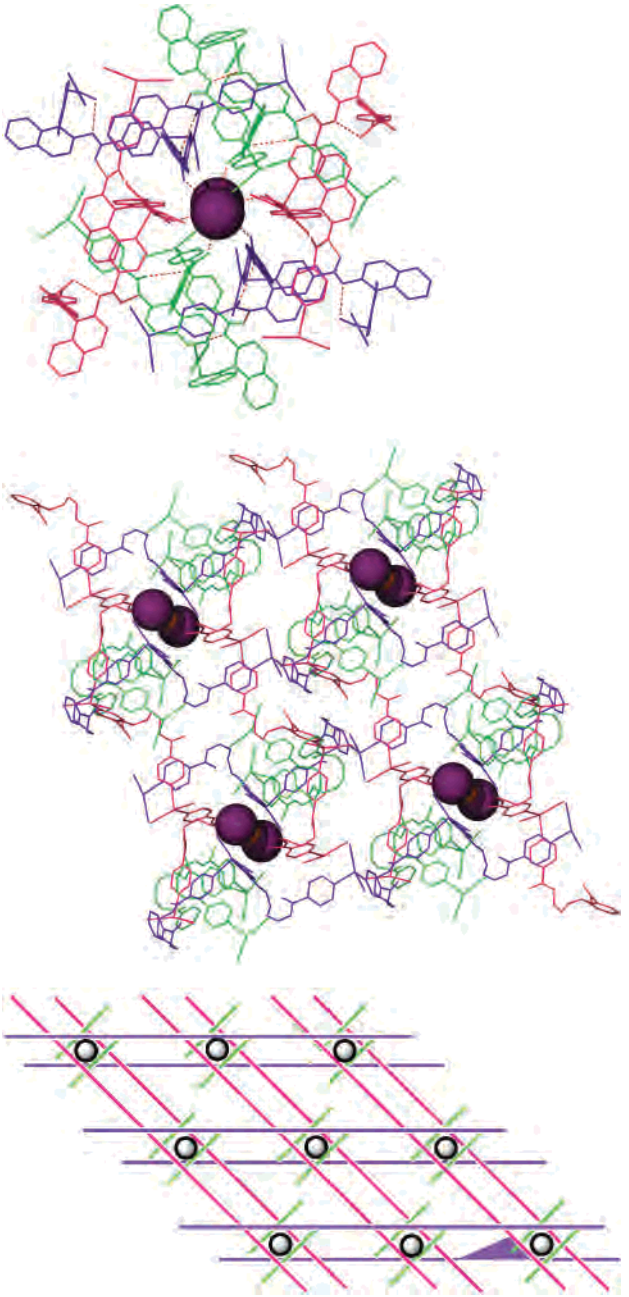

Figure 9. Solid-state structure of complex **7c**. (Top) View showing six polymer chains organized around a free HgI_2 template. (Middle) View of the three-dimensional grid network (naphthyl rings have been removed for clarity). (Bottom) Drawing representing the grid structure formed around free HgI_2 molecules.

Table 5. Selected Bond Distances (Å) and Angles (deg) for the Three-Dimensional Network **7c**

Hg(1)−N(1)	2.447(15)	N(8A)−Hg(1)−X(1)	101(5)
Hg(1)−N(8A)	2.44(17)	N(1)−Hg(1)−X(2)	104.8(4)
Hg(1)−X(1)	2.6196(19)	N(8A)−Hg(1)−X(2)	104(5)
Hg(1)−X(2)	2.635(3)	X(1)−Hg(1)−X(2)	145.83(11)
Hg(2)−N(4)	2.442(10)	N(4)−Hg(2)−N(5)	82.8(5)
Hg(2)−N(5)	2.509(11)	N(4)−Hg(2)−X(3)	103.2(4)
Hg(2)−X(3)	2.651(2)	N(4)−Hg(2)−X(4)	100.7(4)
Hg(2)−X(4)	2.640(2)	N(5)−Hg(2)−X(3)	97.8(4)
Hg(3)−I(5)/(5A)	2.575(7)	N(5)−Hg(2)−X(4)	104.6(4)
N(1)−Hg(1)−N(8A)	82(4)	X(3)−Hg(2)−X(4)	148.99(9)
N(1)−Hg(1)−X(1)	101.3(4)	X(5)−Hg(3)−X(5A)	180.0

^{1}H NMR spectra of the 3-pyridyl complexes **5** (Table S1, Supporting Information). The data show that there is an interaction with the added mercury(II) halide, but they do not define its nature. The complexes were insufficiently soluble to allow low-temperature NMR spectra to be obtained.

Chart 2. ^{1}H NMR Labeling Scheme.

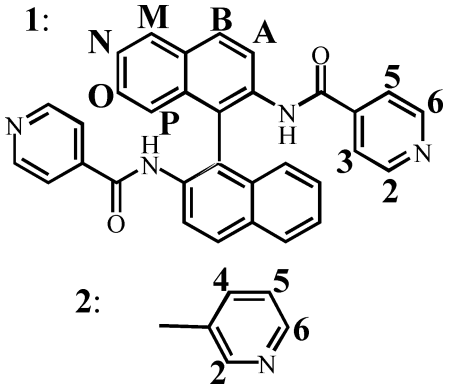

Table 6. Chemical Shifts (ppm) of the ^{1}H NMR Resonances of the 4-Pyridyl Compounds **1**, **3**, and **4** in CD_2Cl_2

	2, 6	A	B	M	NH	N	O	P	3, 5
rac/R-**1**	8.49	8.36	8.13	8.00	8.01	7.50	7.33	7.19	7.04
3a	8.54	8.37	8.15	8.03	7.96	7.53	7.37	7.22	7.15
3b	8.54	8.37	8.15	8.03	7.96	7.53	7.37	7.22	7.16
3c	8.54	8.37	8.15	8.02	7.96	7.53	7.37	7.22	7.15
4c	8.57	8.35	8.15	8.03	8.00	7.53	7.36	7.21	7.21
3a + x$HgCl_2$	8.58	8.31	8.16	8.03	8.01	7.53	7.37	7.26	7.21
3b + x$HgBr_2$	8.61	8.29	8.16	8.03	8.02	7.54	7.37	7.33	7.21
3c + xHgI_2	8.60	8.30	8.16	8.03	8.02	7.53	7.37	7.26	7.20
4c + xHgI_2	8.59	8.31	8.15	8.02	8.02	7.53	7.36	7.26	7.20

Because the complexes, and the free mercury(II) halides, have limited solubility in CD_2Cl_2, the ^{1}H NMR spectra of the 1:1 complexes were also recorded in a 50:50 mixture of CD_2Cl_2 and methanol-d_4, which is a better solvent system. At room temperature, the resonances corresponding to the pyridyl protons H(2) and H(6) were very broad, as shown for complex **3b** in Figure 10, suggesting fluxionality between isomers or oligomers in solution. As the temperature was lowered, these pyridyl proton resonances sharpened and most of the intensity was contained in a single peak at −90 °C. These limited data indicate that fluxionality is slowed and that the equilibrium is shifted to favor one isomer at low temperatures (Figure 10).

The ^{1}H NMR spectra of the complexes in CD_2Cl_2/methanol-d_4 solution at room temperature in the presence of

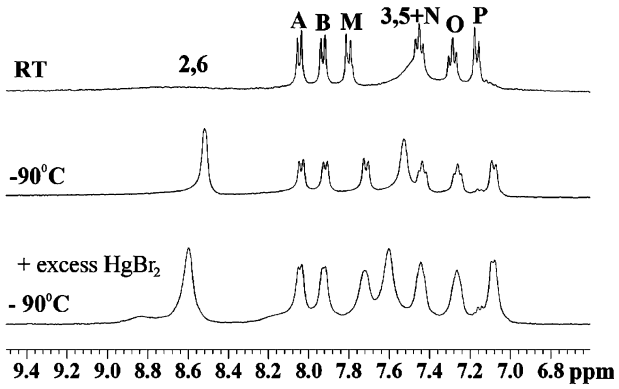

Figure 10. ^{1}H NMR spectra of complex **3b** in 50:50 CD_2Cl_2/methanol-d_4 at room temperature, −90 °C, and with excess $HgBr_2$ added at −90 °C.

excess mercury(II) halide again contained broad pyridyl proton resonances that sharpened as the temperature was lowered to −90 °C (Figure 10). There were other low-intensity broad resonances in the low-temperature spectra (Figure 10). When extra ligand was added to the solution, the chemical shifts of the proton resonances shifted back to the values found for the 1:1 complex.

Discussion

Bridging bis(pyridyl) ligands are often used in the construction of metal-containing macromolecules, and the geometry and flexibility of the bis(pyridyl) ligand can be important in defining the primary structure of the self-assembled macromolecule. The incorporation of chiral binaphthyl units into the bis(amidopyridyl) ligands gave the new ligands **1** and **2** a natural helicity that was retained in complexes **3**−**7** and led to the formation of nonlinear polymers and macrocycles. The binaphthyl bis(amidopyridyl) ligands **1** and **2** have a somewhat rigid conformation at the binaphthyl center, but there is limited rotation about the C−C bond to form complexes with a range of torsion angles = 86.8−106.7° between the naphthyl groups. There is more flexibility of the ligands at the amide groups, and this ligand flexibility together with the evident lability of the Hg−N bonds allows easy interconversion between isomers and oligomers in solution. The ^{1}H NMR spectra of complexes **3**−**5** in CD_2Cl_2 solution at room temperature were simple, probably because there is rapid exchange under these conditions. The NMR spectra in the more polar, mixed solvent system CD_2Cl_2/methanol-d_4 could be measured over a wider temperature range and gave more evidence for a dynamic exchange between different mercury complexes in solution, though the nature of the complexes was not defined. Attempts were made to determine the degree of oligomerization of the complexes in solution by electrospray ionization mass spectrometry, but the complexes are neutral and failed to give useful data even in the presence of formic acid or alkali metal halides to aid ionization.

In contrast to the uncertain solution-state structures of the complexes, several of the solid-state structures are clearly established by X-ray structure determinations. The 1:1 4-pyridyl complexes **3** and **4** crystallize as polymers, but with several different structural motifs, whereas the 1:1 3-pyridyl complexes **5** crystallize as macrocycles. Complexes $[HgX_2(\mu\text{-}rac\text{-}\mathbf{1})]_n$, **3a** (X = Cl) and **3b** (X = Br), formed homochiral polymers containing equal numbers of chains with only *R*-**1** or only *S*-**1** bridging ligands. Complex **3a** was crystallized in two forms, one containing zigzag chains (polymer **3a***, Figure 2) and the other with helical chains (polymer **3a****, Figure 3). In contrast, complex $[HgI_2(\mu\text{-}rac\text{-}\mathbf{1})]_n$, **3c**, formed a heterochiral polymer with alternating *R*-**1** and *S*-**1** bridging ligands in each polymer chain (Figure 4). The heterochiral polymeric structure is retained in the HgI_2 inclusion compound **7c** (Figure 9), though the arrangement of the polymer chains is greatly affected by the mercury(II) iodide "guest" molecule. A more dramatic effect is observed in the HgX_2 inclusion compounds with X = Br or I, when a transformation from a homochiral polymer in the 1:1 complexes **3a** and **3b** to a heterochiral macrocycle in the HgX_2 inclusion complexes **6b** and **6c** is observed (Figure 7). Complex **4c**, $[HgI_2(\mu\text{-}R\text{-}\mathbf{1})]_n$, formed a helical polymer and was the only enantiopure structure obtained (Figure 5). Complexes **5a** (X = Cl) and **5b** (X = Br) formed heterochiral macrocycles $[(HgX_2)_2(\mu\text{-}R\text{-}\mathbf{2})(\mu\text{-}S\text{-}\mathbf{2})]$ (Figure 6) rather than polymers, as in the analogous 4-pyridyl complexes **3** and **4**, and clearly, in the absence of excess mercury(II) halide, the 4-pyridyl ligand **1** favors polymer formation, whereas the 3-pyridyl ligand **2** favors the formation of macrocycles.

In summary, the self-assembly of mercury(II) halides with the racemic form of ligands **1** and **2** can give polymers or macrocycles, and the adjacent ligands can have the same or opposite chirality. It is likely that solutions of the complexes contain oligomers and macrocycles in easy equilibrium, that the position of the equilibrium is both solvent- and temperature-dependent and also affected by template effects with added mercury(II) halide, and that the oligomers contain both homochiral and heterochiral sequences. The more selective self-assembly occurs during crystallization, but the compound that crystallizes will clearly be affected by the solution equilibria as well as by the relative solubilities of the homochiral and heterochiral polymers and the macrocycles.

In all of the complexes studied, amide hydrogen bonding was important in organizing the polymers and macrocycles into ordered networks in the solid state. In each complex, one N−H and C═O pair of each ligand formed an intraligand hydrogen bond, leaving one N−H and C═O group of each ligand free for intermolecular hydrogen bonding with ligands of other molecules. In the majority of complexes, the intermolecular hydrogen bonding occurred between ligands of opposite chirality (···*R*···*S*···), but in complex **3c**, the hydrogen bonding was between ligands of like chirality (···*R*···*R*···, ···*S*···*S*···).

The high selectivity of the self-assembly process in the solid state when a racemic form of a chiral ligand is one component is impressive, because it involves self-recognition or self-discrimination in selecting neighboring ligands, selective formation of open or cyclic units, and selective association through hydrogen bonding. Clearly, the overall racemic networks formed could not be formed by the use of enantiopure ligands.

Experimental Section

NMR spectra were recorded using a Varian Inova 400 NMR spectrometer. ^{1}H and ^{13}C chemical shifts are reported relative to tetramethylsilane. The NMR labeling is defined in Chart 2. The synthesis of *rac*-**2** was described previously.[8]

I. Synthesis. A. *rac*-1,1′-$C_{10}H_{12}$-2,2′-[NHC(═O)-4-C_5H_4N]$_2$, *rac*-1. Triethylamine (2.8 mL, 20.4 mmol) and a solution of *rac*-2,2′-diamino-1,1′-binaphthyl (2.20 g, 7.7 mmol) in THF (30 mL) were added to a suspension of isonicotinoyl chloride hydrochloride (3.56 g, 20.0 mmol) in THF (30 mL), and the mixture was heated to reflux for 8 h. After the mixture was cooled, the volume of THF was reduced by rotary evaporation and the mixture was poured into ice water. The product was collected by vacuum filtration, washed with cold water and acetone, and dried under a vacuum. Yield: 2.61 g, 73%. ^{1}H NMR (CD_2Cl_2): 8.49 (d, $^3J_{HH}$ = 6 Hz, 4H, $H^{2,6}$ py), 8.36 (d, $^3J_{HH}$ = 9 Hz, 2H, H^B), 8.13 (d, $^3J_{HH}$ = 9 Hz,

2H, H^M), 8.01 (m, 4H, H^A, NH), 7.50 (t, $^3J_{HH}$ = 8 Hz, 2H, H^N), 7.33 (t, $^3J_{HH}$ = 8 Hz, 2H, H^O), 7.20 (d, $^3J_{HH}$ = 8 Hz, 2H, H^P), 7.09 (d, $^3J_{HH}$ = 6 Hz, 4H, $H^{3,5}$ py). MS *m*/*z*: calcd, 494.1742; found, 494.1737.

B. *R*-1,1′-$C_{10}H_{12}$-2,2′-[NHC(=O)-4-C_5H_4N]$_2$, *R*-1. This was prepared similarly to the method described above from triethylamine (0.4 mL, 2.9 mmol), *R*-2,2′-diamino-1,1′-binaphthyl (0.40 g, 1.4 mmol), and isonicotinoyl chloride hydrochloride (2.8 mmol, 0.498 g). Yield: 0.264 g, 40%. NMR as for *rac*-**1**. MS *m*/*z*: calcd, 494.1742; found, 494.1742.

C. [{HgCl$_2$(*μ*-*rac*-1)}$_x$], 3a. $HgCl_2$ (0.0406 g, 0.150 mmol) was added to a stirring solution of *rac*-**1** (0.0741 g, 0.150 mmol) in CH_2Cl_2, and immediate precipitation of a white solid was observed. The mixture was allowed to stir for an additional 30 min to complete precipitation, then the product was collected by vacuum filtration and dried under a vacuum. Yield: 0.0656 g, 60%. ^{1}H NMR (CD_2Cl_2): 8.53 (d, $^3J_{HH}$ = 6 Hz, 4H, $H^{2,6}$ py), 8.37 (d, $^3J_{HH}$ = 9 Hz, 2H, H^B), 8.14 (d, $^3J_{HH}$ = 9 Hz, 2H, H^M), 8.02 (d, $^3J_{HH}$ = 8 Hz, 2H, H^A), 7.92 (s, 2H, NH), 7.52 (t, $^3J_{HH}$ = 8 Hz, 2H, H^N), 7.35 (t, $^3J_{HH}$ = 8 Hz, 2H, H^O), 7.20 (d, $^3J_{HH}$ = 8 Hz, 2H, H^P), 7.14 (d, $^3J_{HH}$ = 6 Hz, 4H, $H^{3,5}$ py). Anal. Calcd for $C_{32}H_{22}N_4O_2HgCl_2$: C, 50.44; H, 2.38; N, 7.35. Found: C, 50.21; H, 2.68; N, 7.37%.

D. [{HgBr$_2$(*μ*-*rac*-1)}$_x$], 3b. This was prepared similarly to the method described for **3a** from $HgBr_2$ (0.0540 g, 0.150 mmol) and *rac*-**1** (0.0741 g, 0.150 mmol). Yield: 0.0834 g, 67%. ^{1}H NMR (CD_2Cl_2): 8.55 (d, $^3J_{HH}$ = 5 Hz, 4H, $H^{2,6}$ py), 8.37 (d, $^3J_{HH}$ = 9 Hz, 2H, H^B), 8.16 (d, $^3J_{HH}$ = 9 Hz, 2H, H^M), 8.03 (d, $^3J_{HH}$ = 9 Hz, 2H, H^A), 7.95 (s, 2H, NH), 7.53 (t, $^3J_{HH}$ = 8 Hz, 2H, H^N), 7.37 (t, $^3J_{HH}$ = 8 Hz, 2H, H^O), 7.22 (d, $^3J_{HH}$ = 8 Hz, 2H, H^P), 7.16 (d, $^3J_{HH}$ = 5 Hz, 4H, $H^{3,5}$ py). Anal. Calcd for $C_{32}H_{22}N_4O_2HgBr_2$: C, 45.17; H, 2.13; N, 6.58. Found: C, 44.96; H, 2.29; N, 6.61%.

E. [{HgI$_2$(*μ*-*rac*-1)}$_x$], 3c. This was prepared similarly to the method described for **3a** from HgI_2 (0.0681 g, 0.150 mmol) and *rac*-**1** (0.0741 g, 0.150 mmol). Yield: 0.0991 g, 70%. ^{1}H NMR (CD_2Cl_2): 8.55 (d, $^3J_{HH}$ = 5 Hz, 4H, $H^{2,6}$ py), 8.37 (d, $^3J_{HH}$ = 9 Hz, 2H, H^B), 8.16 (d, $^3J_{HH}$ = 9 Hz, 2H, H^M), 8.02 (d, $^3J_{HH}$ = 9 Hz, 2H, H^A), 7.95 (s, 2H, NH), 7.53 (t, $^3J_{HH}$ = 8 Hz, 2H, H^N), 7.37 (t, $^3J_{HH}$ = 8 Hz, 2H, H^O), 7.22 (d, $^3J_{HH}$ = 8 Hz, 2H, H^P), 7.15 (d, $^3J_{HH}$ = 5 Hz, 4H, $H^{3,5}$ py). Anal. Calcd for $C_{32}H_{22}N_4O_2HgI_2$: C, 40.68; H, 1.92; N, 5.93. Found: C, 40.22; H, 2.07; N, 5.91%.

F. [{HgI$_2$(*μ*-*R*-1)}$_x$], 4c. This was prepared similarly to the method described for **3a** from HgI_2 (0.0681 g, 0.150 mmol) and *R*-**1** (0.0741 g, 0.150 mmol). Yield: 0.0940 g, 67%. ^{1}H NMR (CD_2Cl_2): 8.57 [s (br), 4H, $H^{2,6}$ py], 8.35 (d, $^3J_{HH}$ = 9 Hz, 2H, H^B), 8.15 (d, $^3J_{HH}$ = 9 Hz, 2H, H^M), 8.03 (d, $^3J_{HH}$ = 8 Hz, 2H, H^A), 8.00 (s, 2H, NH), 7.53 (t, $^3J_{HH}$ = 8 Hz, 2H, H^N), 7.36 (t, $^3J_{HH}$ = 8 Hz, 2H, H^O), 7.21 (m, 6H, H^P, $H^{3,5}$ py). Anal. Calcd for $C_{32}H_{22}N_4O_2HgI_2$: C, 40.68; H, 1.92; N, 5.93. Found: C, 40.35; H, 2.34; N, 6.31%.

G. [(HgCl$_2$)$_2$(*μ*-*R*-2) (*μ*-*S*-2)], 5a. This was prepared similarly to the method described for **3a** from $HgCl_2$ (0.0406 g, 0.150 mmol) and *R*-**2** (0.0741 g, 0.150 mmol). Yield: 0.0914 g, 83%. ^{1}H NMR (CD_2Cl_2): 8.58 (d, $^3J_{HH}$ = 6 Hz, 2H, H^6 py), 8.49 (s, 2H, H^2 py), 8.35 (d, $^3J_{HH}$ = 9 Hz, 2H, H^A), 8.12 (d, $^3J_{HH}$ = 9 Hz, 2H, H^B), 8.00 (d, $^3J_{HH}$ = 8 Hz, 2H, H^M), 7.93 (s, 2H, NH), 7.71 (d, $^3J_{HH}$ = 6 Hz, 2H, H^4 py), 7.50 (t, $^3J_{HH}$ = 8 Hz, 2H, H^N), 7.34 (t, $^3J_{HH}$ = 8 Hz, 2H, H^O), 7.25 (m, 2H, H^5 py), 7.19 (d, $^3J_{HH}$ = 8 Hz, 2H, H^P). Anal. Calcd for $C_{32}H_{22}N_4O_2HgCl_2$: C, 50.44; H, 2.38; N, 7.35. Found: C, 49.99; H, 2.58; N, 7.11%.

H. [(HgBr$_2$)$_2$(*μ*-*R*-2)(*μ*-*S*-2)], 5b. This was prepared similarly to the method described for **3a** from $HgBr_2$ (0.0540 g, 0.150 mmol) and *R*-**2** (0.0741 g, 0.150 mmol). Yield: 0.0909 g, 73%. ^{1}H NMR (CD_2Cl_2): 8.59 (d, $^3J_{HH}$ = 6 Hz, 2H, H^6 py), 8.49 (s, 2H, H^2 py), 8.35 (d, $^3J_{HH}$ = 9 Hz, 2H, H^A), 8.13 (d, $^3J_{HH}$ = 9 Hz, 2H, H^B), 8.00 (d, $^3J_{HH}$ = 8 Hz, 2H, H^M), 7.93 (s, 2H, NH), 7.71 (d, $^3J_{HH}$ = 6 Hz, 2H, H^4 py), 7.50 (t, $^3J_{HH}$ = 8 Hz, 2H, H^N), 7.34 (t, $^3J_{HH}$ = 8 Hz, 2H, H^O), 7.26 (m, 2H, H^5 py), 7.19 (d, $^3J_{HH}$ = 8 Hz, 2H, H^P). Anal. Calcd for $C_{32}H_{22}N_4O_2HgBr_2$: C, 45.17; H, 2.13; N, 6.58. Found: C, 44.98; H, 2.27; N, 6.38%.

II. X-ray Structure Determinations. Crystals were mounted on glass fibers. Data were collected at 150 K using a Nonius-Kappa CCD diffractometer using COLLECT (B. V. Nonius, 1998) software. No significant decay occurred during data collection at this temperature, though easy solvent loss occurred at room temperature. The unit cell parameters were calculated and refined from the full data set. Crystal cell refinement and data reduction were carried out using the Nonius DENZO package. The data were scaled using SCALEPACK (B. V. Nonius, 1998). The SHELX-TL V5.1 and SHELX-TL V6.1 (G. M. Sheldrick) program packages were used to solve and refine the structures. The structures were solved by direct methods, except for **5a**, which was solved by the automated Patterson routine. Except as mentioned, all non-hydrogen atoms were refined with anisotropic thermal parameters. The hydrogen atoms were calculated geometrically and were riding on their respective carbon atoms. Thermal ellipsoid diagrams are shown at 30% probability. Crystal data are summarized in Tables 7 and 8.

A. *rac*-1,1′-$C_{10}H_{12}$-2,2′-[NHC(=O)-4-C_5H_4N]$_2$, *rac*-1. Crystals of *rac*-(±)-$C_{32}H_{22}N_4O_2$·THF were grown from the diffusion of hexane into a tetrahydrofuran/methanol solution of the complex. The THF solvent molecule was disordered and was modeled as a 55:25:20 isotropic mixture with geometric restraints. The largest residual electron density peak (0.347 e/Å^3) was associated with the THF solvent molecule.

B. [{HgCl$_2$(*μ*-*rac*-1)}$_x$], 3a*. Crystals of *rac*-(±)-[$C_{32}H_{22}Cl_2HgN_4O_2$]·CH_2Cl_2 were grown from the diffusion of hexane into a CH_2Cl_2/methanol solution of the complex. The CH_2Cl_2 solvent molecule was disordered and was modeled as a 30:35:35 isotropic mixture with geometric restraints. The largest residual electron density peak (3.26 e/Å^3) was associated with the CH_2Cl_2 solvent molecule.

C. [{HgCl$_2$(*μ*-*rac*-1)}$_x$], 3a.** Crystals of *rac*-(±)-[$C_{32}H_{22}Cl_2HgN_4O_2$]·CH_2Cl_2 were grown from the diffusion of hexane into a CH_2Cl_2/methanol solution of the complex. The largest residual electron density peak (1.373 e/Å^3) was associated with the C(l4) atom.

D. [{HgBr$_2$(*μ*-*rac*-1)}$_x$], 3b. Crystals of *rac*-(±)-[$C_{32}H_{22}Br_2HgN_4O_2$]·CH_2Cl_2 were grown from the diffusion of hexane into a CH_2Cl_2/methanol solution of the complex. The CH_2Cl_2 solvent molecule was disordered and was modeled as a 70:30 mixture. The largest residual electron density peak (1.371 e/Å^3) was associated with the Br(1) atom.

E. [{HgI$_2$(*μ*-*rac*-1)}$_x$], 3c. Crystals of *rac*-(±)-[$C_{32}H_{22}HgI_2N_4O_2$]·2.25(CH_2Cl_2) were grown from the diffusion of hexane into a CH_2Cl_2/methanol solution of the complex. One of the CH_2Cl_2 solvent molecules, which laid on a symmetry element, was modeled at 50% occupancy with isotropic thermal parameters. The largest residual electron density peak (3.039 e/Å^3) was associated with the I(2) atom.

F. [{HgI$_2$(*μ*-*R*-1)}$_x$], 4c. Crystals of (*R*)-(+)-[$C_{32}H_{22}HgI_2N_4O_2$]·{CH_2Cl_2}{$O(CH_3CH_2)_2$} were grown from the diffusion of diethyl ether into a CH_2Cl_2/methanol solution of the complex. The Flack parameter refined to a value of 0.0385(8), indicating the correct hand of the molecule was refined. The largest residual electron density peak (1.539 e/Å^3) was associated with the mercury atom.

G. [(HgCl$_2$)$_2$(*μ*-*R*-2)(*μ*-*S*-2)], 5a. Crystals of *rac*-(±)-[$C_{32}H_{22}Cl_2HgN_4O_2$]·0.4(CH_2Cl_2)0.6(CH_3OH) were grown from the diffu-

Table 7. Crystallographic Data for Complexes *rac*-**1**, **3a***, **3a****, **3b**, **3c**, and **4c**

	1·THF	**3a***·CH_2Cl_2	**3a****·CH_2Cl_2
formula	$C_{36}H_{30}N_4O_3$	$C_{33}H_{24}Cl_{4.5}HgI_2N_4O_2$	$C_{33}H_{24}Cl_4HgN_4O_2$
fw	566.64	850.95	850.95
space group	*P*2(1)/*c*	*P*2(1)/*n*	*P*2(1)/*c*
a (Å)	9.5809(19)	10.188(2)	17.124(3)
b (Å)	18.196(4)	22.928(5)	11.727(2)
c (Å)	17.263(4)	13.624(3)	16.249(3)
a (deg)	90	90	90
b (deg)	105.54(3)	93.11(3)	103.84(3)
g (deg)	90	90	90
V(Å^3)	2899.3(10)	3177.8(11)	3168.2(11)
Z	4	4	4
D_{calc} (mg/m^3)	1.298	1.779	1.784
μ (mm^{-1})	0.084	5.217	5.233
R1, wR2 [I >2σ(I)]	0.0574, 0.1497	0.0413, 0.1103	0.0432, 0.0840
R indices (all data)	0.1053, 0.1667	0.0607, 0.1170	0.0920, 0.0983

	3b·CH_2Cl_2	**3c**·2.25(CH_2Cl_2)	**4c**·{CH_2Cl_2}{$O(CH_3CH_2)_2$}
formula	$C_{33}H_{24}Br_4HgN_4O_2$	$C_{34.25}H_{27}Cl_{4.5}HgI_2N_4O_2$	$C_{37}H_{34}Cl_2HgI_2N_4O_3$
fw	939.87	1140.51	1107.97
space group	*P*2(1)/*c*	*C*2/*c*	*P*2(1)2(1)2(1)
a (Å)	17.239(3)	20.856(4)	15.023(3)
b (Å)	11.940(2)	15.847(3)	15.582(3)
c (Å)	16.268(3)	23.865(5)	16.554(3)
a (deg)	90	90	90
b (deg)	103.34(3)	96.91(3)	90
g (deg)	90	90	90
V(Å^3)	3258.2(11)	7830(3)	3874.8(13)
Z	4	8	4
D_{calc} (mg/m^3)	1.916	1.935	1.899
μ (mm^{-1})	7.378	5.851	5.744
R1, wR2 [I >2σ(I)]	0.0426, 0.1016	0.0740, 0.1917	0.0465, 0.1015
R indices (all data)	0.0631, 0.1092	0.1469, 0.2271	0.0689, 0.1097

Table 8. Crystallographic Data for Complexes **5a**, **5b**, **6b**, **6c**, and **7c**

	5a·0.6(CH_3OH)0.4(CH_2Cl_2)	**5b**·CH_2Cl_2	**6b**·0.5(CH_3OH)
formula	$C_{33}H_{25.2}Cl_{2.8}HgN_4O_{2.6}$	$C_{33}H_{22}Br_2Cl_2HgN_4O_2$	$C_{32.5}H_{24}Br_3Hg_{1.5}N_4O_{2.5}$
fw	819.22	937.86	1051.17
space group	*P*2(1)/*c*	*P*2(1)/*c*	*P*2(1)/*c*
a (Å)	18.204(4)	18.187(4)	16.652(3)
b (Å)	10.865(2)	11.165(2)	12.318(3)
c (Å)	16.030(3)	16.286(3)	16.223(3)
a (deg)	90	90	90
b (deg)	91.91(3)	92.50(3)	102.03(3)
g (deg)	90	90	90
V (Å^3)	3168.7(11)	3303.6(11)	3254.4(11)
Z	4	4	4
D_{calc} (mg/m^3)	1.717	1.886	2.145
μ (mm^{-1})	5.132	7.276	10.797
R1, wR2 [I >2σ(I)]	0.0717, 0.1982	0.0514, 0.1331	0.0625, 0.1820
R indices (all data)	0.0884, 0.2111	0.0741, 0.1486	0.0810, 0.1954

	6c·2(CH_3OH)	**7c**·(CH_2Cl_2)·0.17(H_2O)
formula	$C_{34}H_{30}Hg_{1.5}I_3N_4O_4$	$C_{65}H_{46.33}Cl_2Hg_{2.17}I_{4.33}N_8O_{4.17}$
fw	1240.20	2061.51
space group	*C*2/*c*	$R\bar{3}$
a (Å)	34.840(7)	26.836(4)
b (Å)	13.241(3)	26.836(4)
c (Å)	16.423(3)	53.305(11)
a (deg)	90	90
b (deg)	103.28(3)	90
g (deg)	90	120
V (Å^3)	7374(3)	33245(9)
Z	8	18
D_{calc} (mg/m^3)	2.234	1.853
μ (mm^{-1})	8.799	6.426
R1, wR2 [I >2σ(I)]	0.0957, 0.2766	0.0954, 0.2451
R indices (all data)	0.1247, 0.3016	0.1482, 0.2819

sion of hexane into a CH_2Cl_2/methanol solution of the complex. The solvent was disordered and was modeled as a 60:40 mixture of CH_3OH/CH_2Cl_2, and the carbon atoms were refined with isotropic thermal parameters. Because of symmetry, only one-half of the molecule was located on the difference Fourier map. The structure was well-resolved with estimated standard deviations on

the order of 0.0012; however, the R value was large (7.09%) as a result of undefined electron density. The largest residual electron density peak was 7.66 e/Å^3 and was 0.94 Å from the mercury atom. This peak is undoubtedly due to an inadequate absorption correction, as the crystal used for data collection was a large (0.05 × 0.075 × 0.775 mm) rod.

H. [(HgBr$_2$)$_2$(*μ*-*R*-2)(*μ*-*S*-2)], 5b. Crystals of *rac*-(±)-[$C_{32}H_{22}Br_2HgN_4O_2$]·CH_2Cl_2 were grown from the diffusion of hexane into a CH_2Cl_2/methanol solution of the complex. The bromine atoms were disordered and were modeled as 55:45 isotropic mixtures. The CH_2Cl_2 solvent molecule, which was centered on a symmetry element, was disordered and was modeled as a 60:40 isotropic mixture with geometric restraints. Because of symmetry, only one-half of the molecule was located on the difference Fourier map. The largest residual electron density peak (1.98 e/Å^3) was associated with the Br(2A) atom.

I. [(HgBr$_2$)$_2$(*μ*-*R*-1)(*μ*-*S*-1)]·HgBr$_2$, 6b. Crystals of *rac*-(±)-[$C_{32}H_{22}Br_3Hg_{1.5}N_4O_2$]·0.5($CH_3OH$) were grown in situ from the diffusion of hexane into a CH_2Cl_2/methanol solution of $C_{32}H_{22}N_4O_2$ and $HgBr_2$. One of the bromine atoms of the molecule was disordered and modeled as a 70:30 mixture. The CH_3OH solvent molecule was modeled at 50% occupancy with isotropic thermal parameters. The molecule laid on a symmetry element. The largest residual electron density peak (3.15 e/Å^3) was associated with the Hg(1) atom.

J. [(HgI$_2$)$_2$(*μ*-*R*-1)(*μ*-*S*-1)]·HgI$_2$, 6c. Crystals of *rac*-(±)-[$C_{32}H_{22}Hg_{1.5}I_3N_4O_2$]·2($CH_3OH$) were grown in situ from the diffusion of hexane into a CH_2Cl_2/methanol solution of $C_{32}H_{22}N_4O_2$ and HgI_2. The I(3) atom was disordered and modeled as a 90:10 mixture. The molecule laid on a symmetry element. The largest residual electron density peak (6.482 e/Å^3) was associated with the Hg(1) atom.

K. {6[(HgI$_2$)$_2$(*μ*-1)$_2$]$_n$·(HgI$_2$)$_n$}, 7c. Crystals of *rac*-(±)-[$C_{64}H_{44}I_{4.33}Hg_{2.17}N_8O_4$]·($CH_2Cl_2$)·0.17($H_2O$) were grown in situ from the diffusion of hexane into a CH_2Cl_2/methanol solution of $C_{32}H_{22}N_4O_2$ and HgI_2. Because of the poor quality of the data, only the Hg, I, N, and O atoms of the main moiety were refined with anisotropic thermal parameters. The I(2) atom was disordered and modeled as a 70:30 mixture. The CH_2Cl_2 solvent molecules were modeled at half occupancy with isotropic thermal parameters. Geometric restraints were applied to some aryl groups. The hydrogen atoms were calculated geometrically and were riding on their respective carbon atoms. The largest residual electron density peak (3.312 e/Å^3) was associated with the Hg(2) atom.

Acknowledgment. We thank the NSERC Canada for financial support and a scholarship to T.J.B. We thank Dr. M. C. Jennings for helpful discussions on the X-ray crystallography results. R.J.P. thanks the Government of Canada for a Canada Research Chair.

Supporting Information Available: Tables of X-ray data in CIF format, NMR data for complexes **2** and **5**, and figures showing thermal ellipsoid plots of the asymmetric units in the crystals are available in electronic form only. This material is available free of charge via the Internet at http://pubs.acs.org.

IC050097W